Efficient Constitutive Model for Continuous Micro-Modeling of Masonry Structures

M. Petracca[a]*, G. Camata[b], E. Spacone[b] and L. Pelà[c]

[a]*ASDEA Software, Pescara, Italy*

[b]*Department of Engineering and Geology (InGeo), Università G.d'Annunzio Chieti e Pescara, Pescara, Italy*

[c]*Department of Civil and Environmental Engineering, Universitat Politècnica de Catalunya (UPC-BarcelonaTech), Barcelona, Spain*

e-mail: m.petracca@asdea.net, https://asdeasoft.net (*corresponding author)

Efficient Constitutive Model for Continuous Micro-Modeling of Masonry Structures

Masonry is a composite material often modeled as an equivalent homogenous material. However, the complexity of its micro-structure leads to complex mechanical responses, which are almost impossible to capture accurately with homogenous constitutive models. Micro-modeling can be used in these scenarios, allowing for the explicit modeling of microstructural components, leading to an accurate capturing of their interaction. Its main drawback is the computational cost, which often makes this approach suitable only for the simulation of small specimens. This is especially true due to strain-softening leading to severe instabilities and non-convergence of the solution. The objective of this work is to propose a simple yet effective constitutive plastic-damage model for the microstructural components of masonry. It is based on a damage model previously developed by the authors. For a better representation of the cyclic response of masonry, plasticity is added using a simplified implementation that does not strictly follow the rules of standard elastoplasticity, allowing an explicit computation of the stress tensor from the strain tensor without the need for an iterative loop at the material level. To reduce the numerical issues related to strain-softening and thus improve the stability of the solution, an IM-PLEX integration algorithm is adopted.

Keywords: masonry; micro-modeling; damage; plasticity; impl-ex; mixed implicit explicit integration; partitioned mesh; parallel computing; seismic analysis; buildings.

Introduction

From a macroscopic standpoint, masonry can be considered a composite material consisting of units (bricks or stones) and mortar joints. Their highly different mechanical properties, dimension ratios, and their arrangement in the microstructure contribute to extremely complex non-linear responses characterized by several different failure mechanisms. Simulation of masonry structures with the Finite Element Method can be done at different levels of detail.

Homogenous continuum models (Pelà, Cervera, and Roca 2011, 2013; Pelà, Cervera, Oller, and Chiumenti 2014) can be used in a standard macroscopic approach, where the whole masonry structure is modeled as an equivalent homogeneous medium equipped with an equivalent homogeneous material that should be able to represent the main features of masonry. This method is the fastest in terms of both computational costs and model complexity. However, simple tensorial constitutive models may not be able to accurately represent features such as strength orthotropy followed by damage-induced anisotropy and the effects of the arrangement and size of micro-structural constituents. Furthermore, it is well known that standard tensorial constitutive models, either based on plasticity, damage, or a combination of them, fail in representing the so-called "size effect" (Barenblatt 2014; Bažant 2004). A "size effect" arises every time a material property does not appear to be the same for two geometrically similar structures with different sizes: In quasi-brittle materials, in fact, both structural brittleness and material strength are found to be scale-dependent.

Other approaches have been proposed in the literature to overcome the shortcomings of macro-modeling in accounting for the effect of the microstructure on the structural response. Fracture-Mechanics has been extensively used to study crack propagation in masonry structures (Accornero, Lacidogna and Carpinteri 2016, 2018; Panian and Yazdani 2020; Yazdani and Habibi 2021). It is able to accurately describe the crack propagation, and the size effects can be captured by resorting to the concepts of scaling laws for strength and brittleness, dimensional analysis and fractal geometry (Carpinteri 1994; Carpinteri and Chiaia 1997; Carpinteri and Puzzi 2009). On the other hand, Continuum-Mechanics has also been used to in this regard. To account for scale effects, the micro-structure should somehow be incorporated into the computational model. This can be achieved either with Micro-Modeling (Drougkas, Pelà and Roca

2014; Lourenço 1996; Lourenço and Rots 1997; Oliveira and Lourenço 2004; Petracca et al. 2017) or with Multi-Scale Computational-Homogenization (Petracca et al. 2016, 2017; Quinteros et al. 2012; Zucchini et al. 2002, 2009; De Bellis 2009; De Bellis et al. 2011; Massart 2003; Massart et al. 2007; Mercatoris, Bouillard and Massart 2009; Mercatoris and Massart 2011).

Among all the aforementioned approaches, this work focuses on Micro-Modeling. Its main advantage is the capability of capturing all the complex failure mechanisms that can appear at the microstructural level, the damage-induced anisotropy, and the interaction between microstructural components, even when simple isotropic tensorial constitutive models are used to model the constitutive behavior of the microscopic components. However, micro-modeling also has some drawbacks that limit its applicability to the simulation of small specimens, making it inapplicable to real-life large-scale structures. When used to model large-scale structures, micro-modeling obviously leads to extremely fine meshes and thus to costly analyses, both in terms of time and computational power. Furthermore, damage growth, strength degradation, and strain localization introduce the extra issue of poor convergence (or even non-convergence at all) even when small time steps are used, increasing the computational cost even more. All the aforementioned drawbacks can be mitigated to a good extent using the right tools, such as parallel computing and robust integration algorithms for the constitutive models.

This work presents a new plastic-damage model as an extension to a continuum damage model previously formulated by the authors (Petracca et al. 2017). The proposed model adds two new aspects to the existing model:

- Plasticity, to represent the inelastic deformation and improve the representation of the masonry response under cyclic loadings. Since the focus of this work is to

propose a fast and robust model for the simulation of large-scale structures, plasticity is introduced in a simplified fashion, avoiding iterative loops inside the constitutive model, thus retaining the explicit evaluation of the stress tensor from the strain tensor as in pure continuum damage models (Saloustros, Cervera, and Pelà, 2018).

- IMPL-EX, a mixed implicit-explicit integration scheme (Oliver, Huespe, and Cante 2008) for the constitutive models that aims at improving the computability and robustness of nonlinear constitutive models showing strain-softening.

All the numerical simulations shown in this work are carried out with the OpenSees (McKenna 2011) solver, where the authors have implemented the proposed constitutive model. Pre- and post-processing are carried out with the STKO software (STKO Scientific ToolKit for OpenSees).

Tension-Compression Plastic-Damage Model

The proposed tension-compression plastic-damage model described herein is an extension of a tension-compression damage model previously formulated by the authors (Petracca et al. 2017), which was in turn based on (Cervera, Oliver and Faria 1995; Wu, Li, and Faria 2006). The original model was formulated in the framework of classical continuum-damage mechanics, and therefore, inelastic permanent deformations were not accounted for, rendering the model unsuitable for simulating structures subjected to cyclic loading. However, a nice feature of continuum-damage models is that they can evaluate the stress tensor explicitly from the strain tensor, without the need for iterative loops at the constitutive level, which is common in the return mapping procedures in plasticity-based models. This makes the constitutive model calculations fast and robust, which is a useful feature when analyzing large-scale structures.

The objective of the proposed new plastic-damage model is to introduce the description of plastic deformations in the existing damage model, keeping the simplicity of the continuum-damage framework. For this reason, plasticity has to be necessarily implemented in a simplified way, such that the stress tensor can still be explicitly evaluated from the strain tensor as per standard continuum-damage models, without introducing iterative procedures at the constitutive level, thus keeping the computational cost of the constitutive response as small as possible.

Constitutive Model

In the following description, all variables without subscripts refer to the current time-step, while those with the n and $n-1$ subscripts refer to the same variables at the two previous (known) time steps.

The nominal stress tensor $\boldsymbol{\sigma}$ is defined as

$$\boldsymbol{\sigma} = (1 - d_c^+)\bar{\boldsymbol{\sigma}}^+ + (1 - d_c^-)\bar{\boldsymbol{\sigma}}^- \tag{1}$$

where $\bar{\boldsymbol{\sigma}}^+$ and $\bar{\boldsymbol{\sigma}}^-$ are the positive and negative parts, respectively, of the effective stress tensor, while d_c^+ and d_c^- are the positive and negative cracking damage variables. They account for stress reduction and stiffness degradation of the effective stress due to the opening of cracks. The effective stress tensor $\bar{\boldsymbol{\sigma}}$ is defined as

$$\bar{\boldsymbol{\sigma}} = \bar{\boldsymbol{\sigma}}^+ + \bar{\boldsymbol{\sigma}}^- \tag{2}$$

$$\bar{\boldsymbol{\sigma}}^{\mp} = \left(1 - {d_{pl}}^{\mp}\right)\tilde{\boldsymbol{\sigma}}^{\mp} \tag{3}$$

where $\tilde{\boldsymbol{\sigma}}^+$ and $\tilde{\boldsymbol{\sigma}}^-$ are the positive and negative parts of the trial (i.e., the elastic prediction) effective stress tensor $\tilde{\boldsymbol{\sigma}}$, while ${d_{pl}}^+$ and ${d_{pl}}^-$ are the positive and negative plastic damage variables that account for stress reduction of the trial effective stress due

to plastic flow. The trial effective stress tensor $\tilde{\boldsymbol{\sigma}}$ is defined as

$$\tilde{\boldsymbol{\sigma}} = \bar{\boldsymbol{\sigma}}_{\boldsymbol{n}} + \boldsymbol{C_0}\colon(\boldsymbol{\varepsilon} - \boldsymbol{\varepsilon_n}) \tag{4}$$

$$\tilde{\boldsymbol{\sigma}}^{+} = \sum_{i=1}^{3}\langle\tilde{\sigma}_i\rangle \boldsymbol{p}_i \otimes \boldsymbol{p}_i \tag{5}$$

$$\tilde{\boldsymbol{\sigma}}^{-} = \tilde{\boldsymbol{\sigma}} - \tilde{\boldsymbol{\sigma}}^{+} \tag{6}$$

where $\bar{\boldsymbol{\sigma}}_{\boldsymbol{n}}$ is the effective stress (i.e., only including plasticity) at the previous time step n, while $\boldsymbol{C_0}\colon(\boldsymbol{\varepsilon} - \boldsymbol{\varepsilon_n})$ is the elastic trial stress increment, $\tilde{\sigma}_i$ is the i^{th} eigenvalue of $\tilde{\boldsymbol{\sigma}}$, and $\boldsymbol{p}_i$ is its associated eigenvector. Note that in equation (4) the elastic trial predictor is performed in an incremental way, while in the standard continuum-damage models the elastic prediction is made in total-strain. Note that equation (4) is equivalent to the more standard format $\tilde{\boldsymbol{\sigma}} = \boldsymbol{C_0}\colon\left(\boldsymbol{\varepsilon} - \boldsymbol{\varepsilon}_{\boldsymbol{p_n}}\right)$, where $\boldsymbol{\varepsilon}_{\boldsymbol{p_n}}$ is the plastic strain tensor at the previous time step n. However, due to the proposed simplified implementation of the plasticity part of the algorithm, the plastic strain tensor does not necessarily need to be computed and stored as an internal variable, so it is more convenient to perform the elastic prediction as in equation (4).

Failure Criteria

The positive and negative failure criteria, or damage surfaces, based on the work of Lubliner et al. (1989), are defined as

$$\tilde{\tau}^{-} = H(-\tilde{\sigma}_{min})\left[\frac{1}{1-\alpha}\left(\alpha\tilde{I}_1 + \sqrt{3\tilde{J}_2} + k_1\beta\langle\tilde{\sigma}_{max}\rangle\right)\right] \tag{7}$$

$$\tilde{\tau}^{+} = H(\tilde{\sigma}_{max})\left[\frac{1}{1-\alpha}\left(\alpha\tilde{I}_1 + \sqrt{3\tilde{J}_2} + \beta\langle\tilde{\sigma}_{max}\rangle\right)\frac{f_t}{f_{cp}}\right] \tag{8}$$

$$\alpha = \frac{k_b - 1}{2k_b - 1} \tag{9}$$

$$\beta = \frac{f_{cp}}{f_t}(1-\alpha) - (1+\alpha) \tag{10}$$

where $\tilde{\tau}^+$ and $\tilde{\tau}^-$ are the so-called equivalent (scalar) positive and negative stresses. $\tilde{I}_1$ is the first invariant of the trial effective stress tensor, $\tilde{J}_2$ is the second invariant of the trial effective deviatoric stress tensor, $\tilde{\sigma}_{max}$ is the maximum trial effective principal stress, f_{cp} is the compressive peak stress, f_t is the tensile strength, and k_b is the ratio of the compressive bi-axial strength to the uniaxial compressive strength. The constant k_1 in equation (7) was proposed by the authors to control the influence the compressive criterion has on the dilatant behavior of the model (see figure (1)). For more information on this aspect, the reader can refer to Petracca et al. (2017).

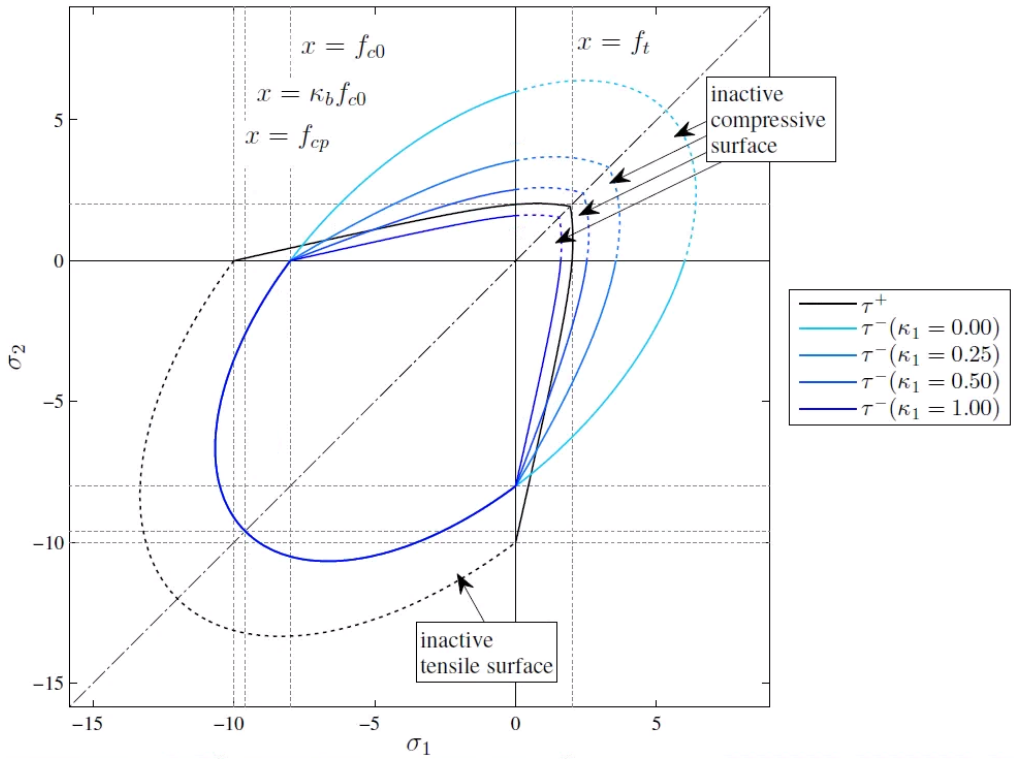

Figure 1. Damage surfaces in the principal stress space (2D plane stress case) (Petracca et al. 2017).

The Heaviside functions of the maximum and minimum eigenvalues, $H(\tilde{\sigma}_{max})$ and $H(-\tilde{\sigma}_{min})$, are required to make sure the compressive surface is active only if at

least one eigenvalue is negative, and, accordingly, the tensile surface is active only if at least one eigenvalue is positive. This is necessary for avoiding tensile damage growth under purely compressive stress states and compressive damage growth under purely tensile stress states. In fact, even if the positive and negative damage variables affect only the associated positive and negative parts of the stress, their failure surfaces, in equations (7) and (8), are a function of the whole stress tensor.

It should also be noted that in equations (7) and (8), the equivalent stresses $\tilde{\tau}^{+}$ and $\tilde{\tau}^{-}$ are functions of the invariants of the trial effective stress tensor $\tilde{\boldsymbol{\sigma}}$, which is computed incrementally as explained before. In this way $\tilde{\tau}^{+}$ and $\tilde{\tau}^{-}$ are not necessarily monotonically increasing variables as required by the continuum-damage framework. To be consistent with the standard continuum-damage framework, the previously computed equivalent stresses are corrected as

$$\tau^{\mp} = \tilde{\tau}^{\mp} + E{\lambda_n}^{\mp} \tag{11}$$

where E is the Young's modulus, and ${\lambda_n}^{+}$ and ${\lambda_n}^{-}$ are the positive and negative equivalent plastic strains, known from the previous time-step. In this way, the equivalent stress measures are like the ones computed in a standard continuum-damage model from the total strain.

Plastic and Cracking damage variables

To impose the irreversibility of the damage process, the model introduces the so-called damage thresholds r^{+} and r^{-}, two scalar variables that denote the largest values ever reached by the equivalent stresses τ^{+} and τ^{-} during the entire loading history for each time step t,

$$r^{+}(t) = \max\left(\underset{s \in [0,t]}{max}\, \tau^{+}(s)\,; f_t\right) \tag{12}$$

$$r^{-}(t) = \max\left(\underset{s \in [0,t]}{max}\, \tau^{-}(s)\,; f_{c0}\right) \tag{13}$$

where f_t and f_{c0} are the elastic limits in tension and compression, respectively. At this point, in view of the last term added in equation (11), r^{+} and r^{-} are two scalar measures of the stress tensor as if they were computed from the total strain. In fact, we can compute their total-strain counterparts and the associated nominal (including the effect of both plasticity and damage) hardening variables, as

$$\varepsilon_{tot}{}^{\mp} = \frac{r^{\mp}}{E} \tag{14}$$

$$q^{\mp} = f^{\mp}\left(\varepsilon_{tot}{}^{\mp}\right) \tag{15}$$

The hardening functions f^{+} and f^{-} of $\varepsilon_{tot}{}^{\mp}$ are reported in figure (3) and figure (3). For a detailed description the reader can refer to Petracca et al.(2017).

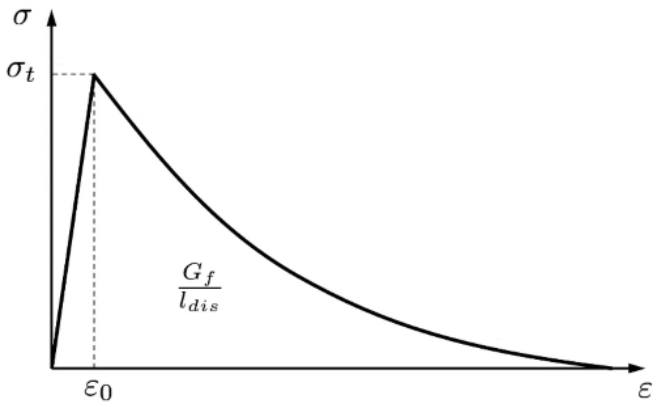

Figure 2. Tensile hardening function

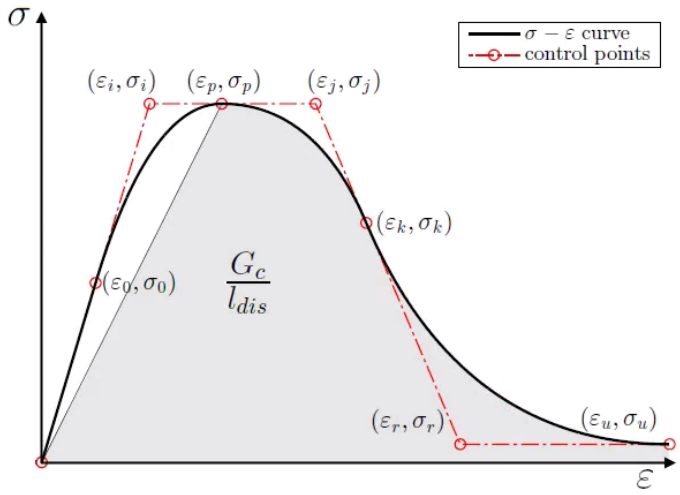

Figure 3. Compressive hardening function

The positive and negative plastic damage variables can be computed as

$$d_{pl}{}^{\mp} = 1 - \frac{q_{pl}{}^{\mp}}{\tilde{r}^{\mp}} \tag{16}$$

$$\tilde{r}^{\mp} = E\left(\varepsilon_{tot}{}^{\mp} - \lambda_n{}^{\mp}\right) \tag{17}$$

$$q_{pl}{}^{\mp} = q^{\mp} + \left(1 - \omega^{\mp}\right)\left(r^{\mp} - q^{\mp}\right) \tag{18}$$

where $\tilde{r}^{\mp}$ are the positive and negative damage thresholds associated with the trial effective stress tensor $\tilde{\boldsymbol{\sigma}}$, $q_{pl}{}^{\mp}$ are the effective (plastic part only) hardening variables, and $\omega^{\mp}$ are the tensile and compressive plastic-damage factors that can be used to calibrate the amount of plasticity to be considered. They range from 0 (pure damage) to 1 (pure plasticity). Once the plastic hardening variables are computed, the cracking damage can be evaluated as

$$d_c^{\mp} = 1 - \frac{q^{\mp}}{q_{pl}{}^{\mp}} \tag{19}$$

With both plastic and cracking damage variables correctly evaluated, the plastic effective stress tensor and the nominal (damaged) stress tensor can be finally calculated as per equations (3) and (1), respectively, and the equivalent plastic strains can be updated as

$$\lambda^{\mp} = {\varepsilon_{tot}}^{\mp} - \frac{{q_{pl}}^{\mp}}{E} \tag{20}$$

A schematic (uniaxial) representation of the above-mentioned process is summarized in figure (4), while figures (5) and (6) show some representative examples of uniaxial and shear tests on a single integration point by varying the magnitudes of $\omega^{\mp}$ factors.

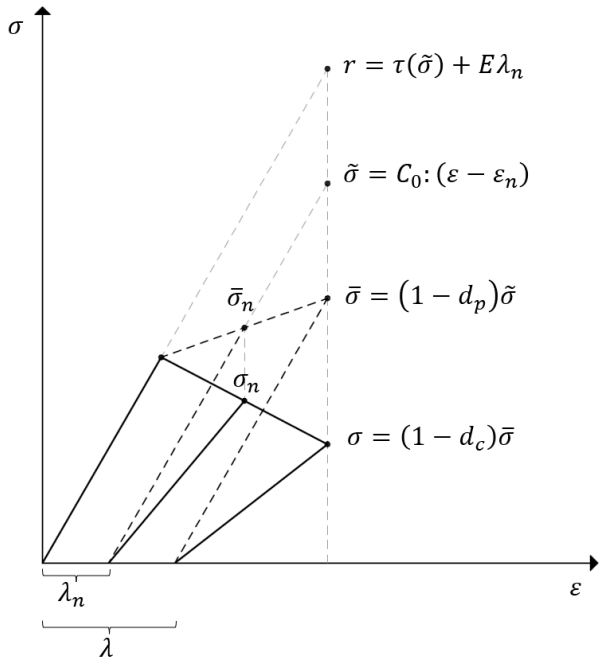

Figure 4. Schematic representation of the elastic predictor and the plastic and damage correctors

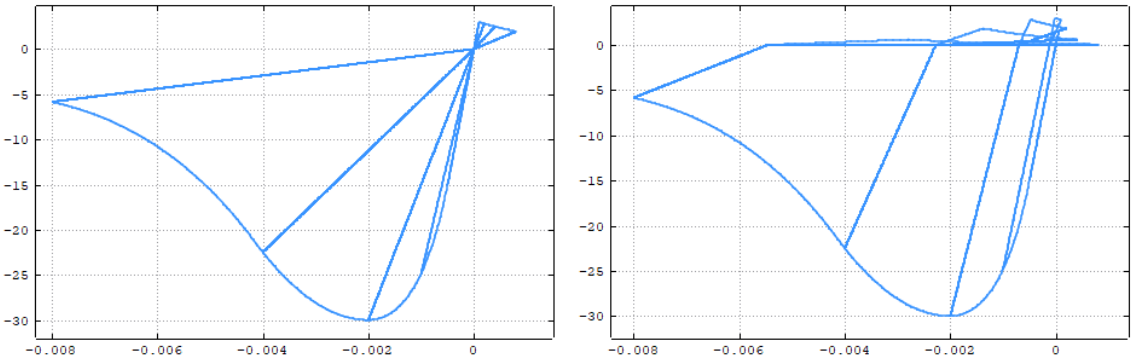

Figure 5. Uniaxial tension-compression cyclic test on one integration point with (a) $\omega^+ = 0$ and $\omega^- = 0.0$, and with (b) $\omega^+ = 0$ and $\omega^- = 0.7$.

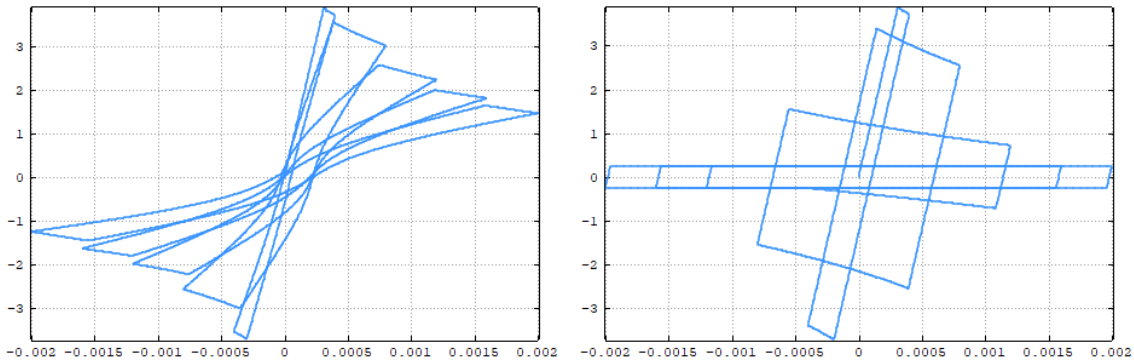

Figure 6. shear cyclic test with a precompression on one integration point with (a) $\omega^+ = 0.5$ and $\omega^- = 0.5$, and with (b) $\omega^+ = 1.0$ and $\omega^- = 1.0$.

Key aspects of the simplified plastic-damage algorithm

As described in the previous sections, the plastic part of the proposed plastic-damage model has been implemented in a simplified fashion, in order to achieve an explicit evaluation of the stress tensor from the current strain tensor, minimizing the number of computations at the constitutive level. Here is a summary of key points of the simplified algorithm:

- Some ingredients of standard plasticity theory, such as yield surface and flow rule, are not present here. Instead, the plastic corrector simply corresponds to an isotropic scaling of the positive and negative parts of the trial elastic stress tensor, as in equation (3) via the plastic-damage variables $d_{pl}{}^{-}$ and $d_{pl}{}^{+}$.
- Plastic ($d_{pl}{}^{\mp}$) and cracking ($d_{c}{}^{\mp}$) damage variables share the same failure criteria in equations (7) and (8), therefore they do not evolve independently.
- How much one damage variable grows with respect to the other is only controlled by the user-defined tensile (ω^{+}) and compressive (ω^{-}) plastic-damage factors. They can range from 0 (only the cracking damage evolves) to 1 (only the plastic damage evolves). For materials such as mortar, the tensile factor can be lower than the compressive one to reflect the more brittle nature of the tensile failure with respect to the compressive failure.

Implementation of the IMPL-EX integration scheme

It is well known that non-linear constitutive models with strain softening lead to instabilities, and the convergence of the iterative procedure becomes difficult to achieve or unachievable. To improve the stability and robustness of this kind of problems, the so-called IMPL-EX integration algorithm originally formulated in Oliver, Huespe, and Cante (2008) is included in the proposed tension-compression plastic-damage model. The IMPL-EX algorithm is a mixed implicit/explicit integration scheme for evaluating the internal variables of a constitutive model. The main idea is that the computation of the constitutive model is divided into two main stages: an explicit extrapolation stage followed by an implicit correction stage.

Explicit Extrapolation

During the global implicit iterative procedure to find equilibrium at time t_{n+1}, the strain tensor is computed in each element, and it is sent to the constitutive model. In the standard integration scheme, the internal variables r^+ and r^- are nonlinear functions of the trial effective stress tensor, as per equations (12) and (13), and therefore, they depend nonlinearly on the current trial strain tensor. This nonlinear dependence makes the global problem nonlinear. The real issue, however, is the presence of strain softening. In this case, the consistent tangent matrix required for the Newton-Raphson scheme may have negative eigenvalues, rendering the global system matrix illconditioned. Instead, in the explicit stage of the IMPL-EX algorithm, those internal variables are linearly extrapolated from the previous values at time t_{n-1} and t_n as

$$r_{n+1}^{\mp} = r_n^{\mp} + \frac{\Delta t_{n+1}}{\Delta t_n}\left(r_n^{\mp} - r_{n-1}^{\mp}\right) \tag{21}$$

In this way, those variables and, in turn, the damage variables depend only linearly on the strain. There is, however, another source of nonlinearity: the tension-compression split of the stress tensor as per equations (5) and (6). Those equations can be re-written after defining the rank-four positive and negative projectors (Pelà, Cervera, and Roca 2011) as follows

$$\boldsymbol{P}^+ = \sum_{i=1}^{3} H(\tilde{\sigma}_i)\boldsymbol{p}_i \otimes \boldsymbol{p}_i \otimes \boldsymbol{p}_i \otimes \boldsymbol{p}_i \tag{22}$$

$$\boldsymbol{P}^- = \boldsymbol{I} - \boldsymbol{P}^+ \tag{23}$$

where $H(\tilde{\sigma}_i)$ is the Heaviside function of the i^{th} principal stress. Now equations (5) and (6) can be re-written as

$$\tilde{\boldsymbol{\sigma}}^{\mp} = \boldsymbol{P}^{\mp} : \tilde{\boldsymbol{\sigma}} \tag{24}$$

In the explicit stage of the IMPL-EX algorithm, those projectors are not computed as a function of the current trial stress but are set equal to their converged values at the previous time step

$$\boldsymbol{P}^{\mp} = \boldsymbol{P}_n^{\mp} \tag{25}$$

At this point, all sources of nonlinearity are removed, and the global problem becomes step-wise linear. Furthermore, the consistent tangent stiffness matrix now coincides with the secant matrix:

$$\boldsymbol{C}^{tan} = \left\{(1-d_c^+)\left(1-d_{pl}^+\right)\mathbf{P}^+ + (1-d_c^-)\left(1-d_{pl}^-\right)\mathbf{P}^-\right\}\!:\boldsymbol{C}_0 \tag{26}$$

Implicit Correction

Once the global implicit iterative procedure has converged and found equilibrium at time t_{n+1}, all the trial internal variables are saved as converged variables, i.e., the starting point for the next time step.

$$r_{n-1}^{\mp} = r_n^{\mp} \tag{27}$$

$$r_n^{\mp} = r^{\mp} \tag{28}$$

$$\lambda_n^{\mp} = \lambda^{\mp} \tag{29}$$

In the IMPL-EX scheme, before doing the aforementioned internal variables swap, a standard implicit update of the current internal variables is performed. This way, the error generated by the explicit extrapolation scheme is mitigated, and due to the nature of the explicit extrapolation, the time-step should be small enough compared to standard implicit schemes to keep the error under control.

Numerical Application

The proposed model, in its original formulation based purely on Continuum-Damage mechanics and a standard implicit integration scheme, has been extensively tested against benchmark problems and small masonry specimens under monotonic loading conditions. In Petracca, Pelà, Rossi, Zaghi, Camata, and Spacone (2017) the model has been first tested in simple 1-element benchmarks to evaluate the shear response against different values of vertical pre-compression both in terms of shear strength and dilatancy, and finally it has been used to simulate experimental tests on the in-plane behavior of small masonry shear walls. Instead, in Petracca, Pelà, Rossi, Oller, Camata, and Spacone (2017), it has been tested against a masonry wall under monotonic out-of-plane actions.

This work, instead, aims at assessing the capability of the new model, equipped with the plasticity part to represent permanent inelastic deformations and a mixed implicit-explicit integration algorithm to improve convergence and stability, to simulate large-scale structures under cyclic loads. A two-story unreinforced masonry (URM) building tested at the University of Pavia, and described in detail in Magenes, Calvi, and Kingsley (1995), is used and simulated numerically to assess the effectiveness and robustness of the proposed plastic-damage model. For a complete description of the model prototype and the testing procedure, the user can refer to Magenes, Calvi, and Kingsley 1(995) and the references therein. Materials were chosen to match typical old urban buildings in Italy, i.e., solid fired-clay bricks with a mean compressive strength on cubes equal to 16 MPa, and mortar made of a mix of hydraulic lime and sand (1:3 volume) with a compressive strength ranging from 2 to 3 MPa. A complete description of material parameters is given in Binda et al. (1995). Material properties for the plastic-damage model used for bricks and mortar joints are given in table (1).

Table 1. Material parameters used in the numerical simulation.

Parameter	Description	Unit	Mortar	Brick
E	Young's modulus	N/mm^2	533.0	2171.0
ν	Poisson's ratio	-	0.15	0.15
f_t	Tensile strength	N/mm^2	0.1	1.62
G_t	Tensile fracture energy	N/mm	0.08	0.1
f_{cp}	Compressive strength at peak	N/mm^2	6.2	6.2
ε_{cp}	Compressive deformation at peak	-	0.015	0.008
G_c	Compressive fracture energy	N/mm	80.0	5.0
k_1	Damage surface: shear compression reduction	-	0.16	0.16
ω^+	Tensile plastic-damage factor	-	0.6	0
ω^-	Compressive plastic-damage factor	-	1.0	0

Note that in the numerical model we used, for both bricks and mortar joints, the compressive strength of the homogenized masonry. This is necessary for 2D and Shell models, due to the plane-stress assumption: Due to the large difference in their elastic constants, when subjected to compressive stress states, mortar is in triaxial-compression (thus increasing its strength against the vertical stress), while brick is in biaxial-tension / uniaxial-compression (thus increasing its strength against the vertical stress). In plane-stress conditions this is not possible, therefore a simple remedy is to use, for both constituents, the compressive strength of the masonry itself.

The structure consists of four components named “Door Wall,” “Window Wall,” and two “Transverse Walls,” subjected to a quasi-static cyclic loading protocol under displacement-control, as shown in figure (7).

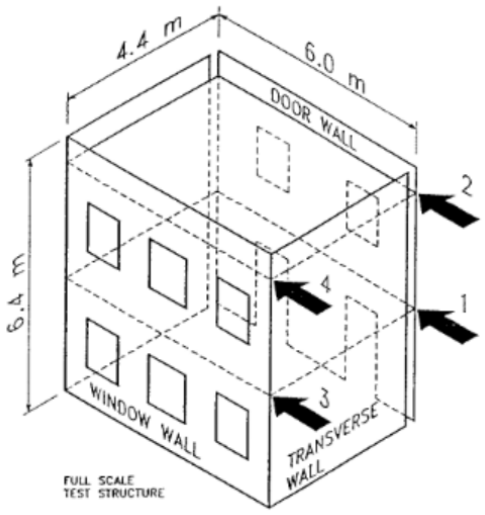

Figure 7: Schematic representation of the tested structure and applied load, taken from Magenes, Calvi, and Kingsley (1995).

The report describes how the Door Wall is substantially detached from the other three walls so that the Window Wall and the two Transverse Walls form a structural system that is almost independent from the Door Wall. There is only a weak coupling represented by the flexible floor steel beams.

The numerical model was created in STKO pre- post-processor (STKO Scientific ToolKit for OpenSees), which automatically produced the TCL input files for the OpenSeesMP parallel solver. OpenSeesMP is a parallel version of OpenSees suitable for running either parallel parametric analysis of small models or a single analysis of a large-scale model. Even if the two structural systems can be efficiently analyzed as two separate 2D analyses due to the weak coupling between them, the objective of this work is to show the performance and robustness of the proposed model in large-scale cyclic analyses. For this reason, we decided to model the whole structure

in a three-dimensional shell model, as shown in figure (8), by discretizing the units and mortar bed/head joints of masonry seperately as is usual in the micro-modeling approach.

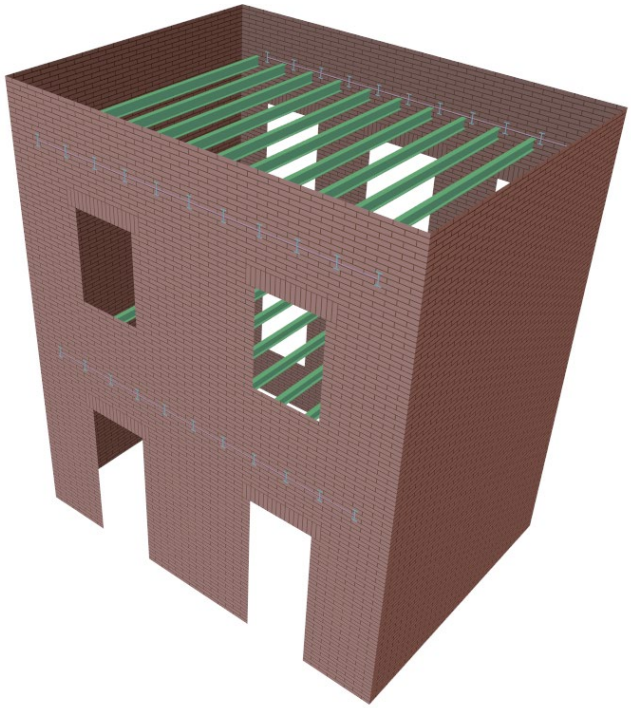

Figure 8: Micro-model developed in STKO's pre andpost-processors

The numerical model consists of 4-node shell elements with a 2 × 2 Gauss integration, five through-the-thickness integration points for bricks and mortar joints, contact elements at the disconnected edges between the Door Walls and the two Transverse Walls, and Force-Based Beam elements for the flexible diaphragm.

The adopted shell element is the ASDShellQ4 (ASDShellQ4 User Manual) element implemented by the authors in OpenSees. The ASDShellQ4 element is a 4-node general purpose thick shell element. The membrane behavior is enhanced with the AGQ6-I (Chen et al. 2004) formulation, which makes the element almost insensitive to geometry distortion, as opposed to standard iso-parametric elements. The drilling DOF (rotation about the normal axis) is treated with the Hughes-Brezzi (Hughes, and Brezzi 1989) formulation, with special care to avoid membrane locking, using a 1 point

quadrature plus hourglass-stabilization. Finally, the plate bending part is treated using the MITC4 (Dvorkin, and Bathe 1984; Bathe, and Dvorkin 1985) formulation to avoid the well known transverse shear locking behavior of thick plate elements.

The model is partitioned into 24 sub-domains to be used with 24 processors in the parallel analysis. The whole mesh consists of roughly 177 thousand elements and 60 thousand nodes, with about 7500 elements per process. The partitioning of the mesh is shown in figure (9).

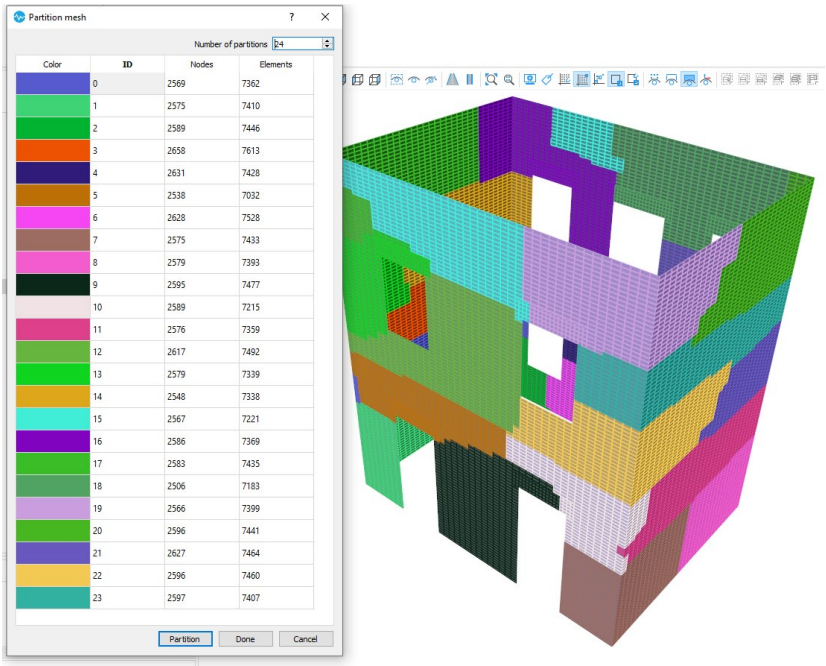

Figure 9: Partitioning of the mesh for parallel computing

The analysis is performed using a Displacement-Control integrator with the cyclic displacement protocol described in Magenes, Calvi, and Kingsley (1995). The imposed displacement-increment for the Displacement-Control integrator is about 2.5 mm, which has proven to be sufficiently small to keep the integration error of the IMPL-EX scheme under an acceptable threshold.

Figure (10) shows the force-displacement curve obtained at the Door Wall, while figure (11) shows the force-displacement curve obtained at the assembly made of

the Window Wall and the two Transverse Walls. The overall prediction of the numerical model is in good agreement with the experimental results, both in terms of maximum force and hysteresis loop. The main difference that can be observed from the two curves is that the numerical model shows more plastic deformations during the first cycles compared to the experimental results. In the experimental results, it seems like the first cycles produce almost only strength and stiffness degradation, while plastic deformations are more predominant during the last cycles. This observation offers a starting point for future work, as in the current implementation the plastic-damage factors ω^+ and ω^- are constant during the analysis. A possible improvement could be an evolutionary law for plastic-damage factors so that the amount of plastic deformations can be controlled over time.

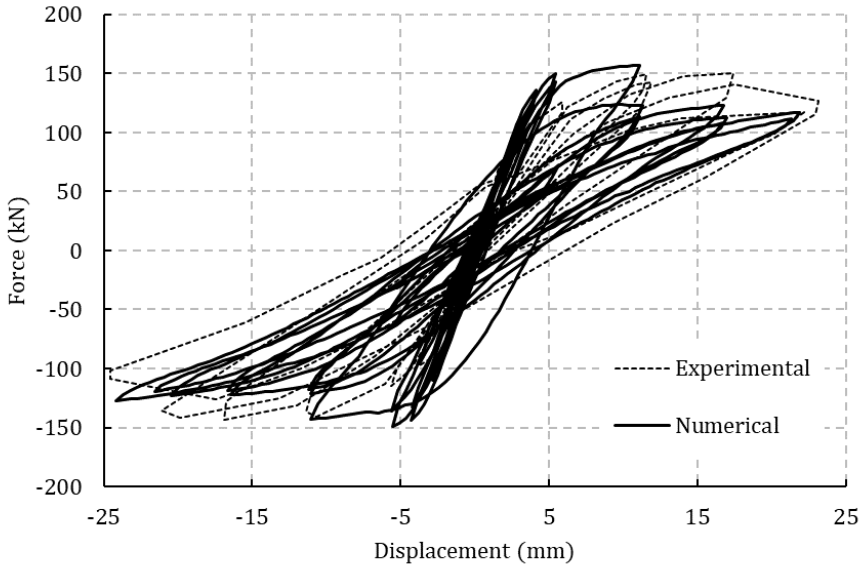

Figure 10: Force-Displacement curve for the Door Wall

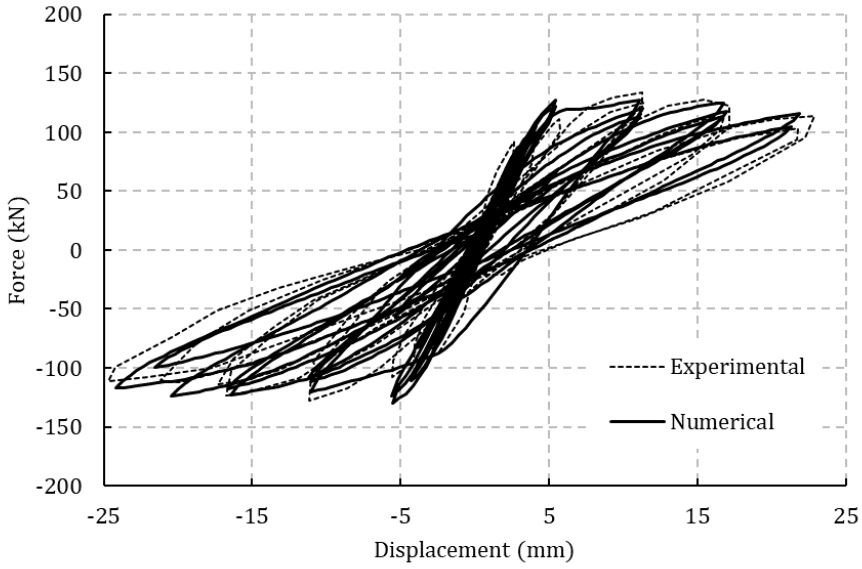

Figure 11: Force-Displacement curve for the Window Wall and the two Transverse Walls

Figures (12) and (13) show the numerically obtained crack pattern at the end of the cyclic analysis, compared with the experimental observations reported in Magenes, Calvi, and Kingsley (1995). The observed failure mechanisms are reproduced satisfactorily.

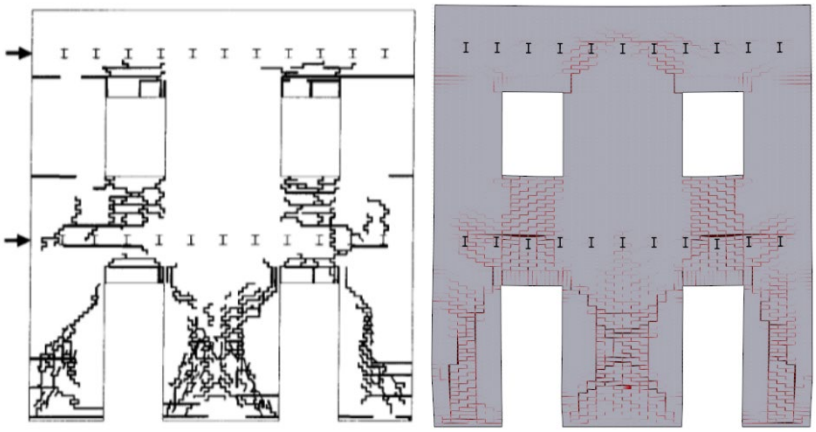

Figure 12: Crack pattern obtained at the end of the analysis for the Door Wall (right), compared with the experimental result (left), taken from Magenes, Calvi, and Kingsley (1995).

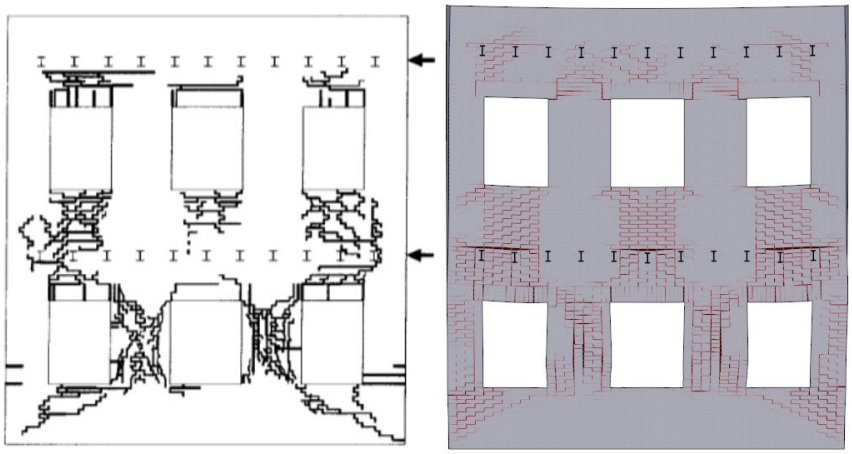

Figure 13: Crack pattern obtained at the end of the analysis for the Window Wall (right), compared with the experimental result (left), taken from Magenes, Calvi, and Kingsley (1995).

Computational Costs

The entire mesh of the case study consists of roughly 177 thousand elements and 60 thousand nodes, 6 DOFs per node, for a total of about 360 thousand equations. The mesh is partitioned into 24 sub-domains and analyzed with OpenSeesMP. The model ran on a 128-cores AMD Ryzen Threadripper 3990X 3.40 GHz CPU. The analysis was subdivided into 3200 time-steps and ran in 2 hours and 53 minutes only, with a constant number of iterations for each time-step equal to 2, thanks to the fact that the IMPL-EX algorithm produces a step-wise linear solution, that is, within each time step, the stress response does not depend on the trial strain. The results in terms of computational time are remarkable and clearly demonstrate the efficiency of the proposed constitutive model combined with a mixed implicit explicit integration algorithm.

Conclusions

This paper presented an efficient constitutive model based on continuum damage

mechanics and improved with the representation of inelastic deformations to better represent the plastic and cyclic response of masonry. The simplified implementation of the inelastic deformations allows an explicit computation of the stress tensor from the input strain tensor without the need for an iterative loop at the material level. The novel constitutive model has been proposed for the continuous micro-modeling of masonry, i.e., by discretizing both units and mortar-joints with continuum finite elements.

Micro-modeling is a tool that can accurately represent the complex nonlinear response of materials such as masonry, with a highly heterogeneous micro-structure where each constituent exhibits strongly nonlinear behavior. The presence of the microstructure in the numerical mesh captures the complex geometric interactions and failure mechanisms that arise at the micro-scale extremely well. Unfortunately, the computational cost is prohibitively high and can drastically increase when standard implicit algorithms are used to solve the nonlinear equations due to the brittle nature of the masonry constituents and, thus the ill conditioning of the system matrix. For this reason, in the literature, micro-modeling has been used mainly for the analysis of small-scale specimens. However, the aforementioned drawbacks can be satisfactorily mitigated by considering parallel computing, as it offers an increase in speed by partitioning the entire domain into many smaller sub-domains that can be analyzed simultaneously. The IMPL-EX algorithm removes the strong nonlinearity given by the plastic-damage model, thus improving convergence and robustness and consequently reducing the computation time. If, as in this case, the only source of nonlinearity is the constitutive model (i.e., other nonlinearities are not considered, such as large deformations), the nonlinear problem becomes step-wise linear, and convergence is guaranteed.

Acknowledgments

The last author gratefully acknowledges the financial support from the Ministry of Science, Innovation and Universities of the Spanish Government (MCIU), the State Agency of Research (AEI), as well as that of the ERDF (European Regional Development Fund) through the project SEVERUS (Multilevel evaluation of seismic vulnerability and risk mitigation of masonry buildings in resilient historical urban centres, ref. num. RTI2018-099589-B-I00).

References

Accornero, F., G. Lacidogna, and A. Carpinteri. 2016. Evolutionary fracture analysis of masonry arches: Effects of shallowness ratio and size scale. *Comptes Rendus Mécanique*, 344:623-630.

Accornero, F., G. Lacidogna, and A. Carpinteri. 2018. Medieval arch bridges in the Lanzo Valleys, Italy: Incremental structural analysis and fracturing benefit. *Journal of Bridge Engineering (ASCE)*, 23(7):05018005.

Accornero, F., G. Lacidogna. 2020. Safety assessment of masonry arch bridges considering the fracturing benefit. *Applied Sciences*, 10:3490.

ASDShellQ4. User Manual, https://opensees.github.io/OpenSeesDocumentation/user/manual/model/elements/ASDShellQ4.html

Barenblatt, G. I. 2014. Flow, deformation and fracture: Lectures on fluid mechanics and the mechanics of deformable solids for mathematicians and physicists. *Cambridge University Press,* 49.

Bathe, K. J., and E. N. Dvorkin. 1985. A four-node plate bending element based on Mindlin/Reissner plate theory and a mixed interpolation. *International Journal for Numerical Methods in Engineering* 21.2:367-383.

Bažant, Z. P. 2004. Scaling theory for quasibrittle structural failure. *Proceedings of the National Academy of Sciences,* 101:13400-13407.

Binda, L., C. Tiraboschi, G. Mirabella Roberti, G. Baronio, and G. Cardani. 1995. Experimental and numerical investigation on a brick masonry building prototype – Measuring masonry material properties: detailed results from an extensive research, Report 5.0. *Dipartimento di Ingegneria Strutturale, Politecnico di Milano.*

Carpinteri, A. 1994. Scaling laws and renormalization groups for strength and toughness of disordered materials. *Int. J. Solids Struct.*, 31:291-302.

Carpinteri, A., and B. Chiaia. 1997. Multifractal scaling laws in the breaking behaviour of disordered materials. *Chaos, Solitons & Fractals*, 135-150.

Carpinteri, A., and S. Puzzi. 2009. he fractal-statistical approach to the size-scale effects on material strength and toughness. *Probabilistic Engineering Mechanics*, 75-83.

Cervera, M., J. Oliver, and R. Faria. 1995. Seismic evaluation of concrete dams via continuum damage models. *Earthquake engineering & structural dynamics*, 24:1225-1245.

Chen, X. M., et al. 2004 Membrane elements insensitive to distortion using the quadrilateral area coordinate method. *Computers & Structures*, 82:35-54.

De Bellis, M. L., and D. Addessi. 2009. A Cosserat based multi-scale technique for masonry structures. *PHD Thesis*.

De Bellis, M. L., and D. Addessi. 2011. A Cosserat based multi-scale model for masonry structures. *International Journal for Multiscale Computational Engineering,* 9.5.

Drougkas, A., L. Pelà, and P. Roca. 2014. Numerical modelling of masonry shear walls failure mechanisms. *Proceedings of 9th International Masonry Conference, Guimarães, Portugal*.

Hughes, T. JR, and F. Brezzi. 1989. On drilling degrees of freedom. *Computer methods in applied mechanics and engineering.* 72.1:105-121

Lourenço, P. B. 1996. Computational strategies for masonry structures. *Ph.D. thesis, TU Delft, Delft University of Technology*

Lourenço, P. B., J. G. and Rots. 1997. Multisurface interface model for analysis of masonry structures. *Journal of engineering mechanics*, 123:660-668.

Lubliner, J., J. Oliver, S. Oller, E. Oñate. 1989. A plastic-damage model for concrete, *International Journal of solids and structures* 25 (3) 299–326.

Magenes, G., G. M. Calvi, and G. R. Kingsley. 1995. Seismic testing of a full-scale, two-story masonry building: Test procedure and measured experimental response. Experimental and numerical investigation on a brick masonry building prototype - numerical prediction of the experiment, Report 3.0. *Gruppo Nazionale La Difesa Dai Terremoti*, University of Pavia, Pavia, Italy.

Massart, T. J. 2003. Multi-scale modeling of damage in masonry structures. *Ph.D. thesis*.

Massart, T. J., R. Peerlings, and M. Geers. 2007. An enhanced multi-scale approach for masonry wall computations with localization of damage. *International Journal for Numerical Methods in Engineering,* 69:1022–1059.

McKenna, F. 2011. OpenSees: a framework for earthquake engineering simulation. *Computing in Science & Engineering*, 13:58-66.

Mercatoris, B., P. Bouillard, and T. Massart. 2009. Multi-scale detection of failure in planar masonry thin shells using computational homogenisation. *Engineering fracture mechanics,* 76: 479–499.

Mercatoris, B., and T. Massart. 2011. A coupled two-scale computational scheme for the failure of periodic quasi-brittle thin planar shells and its application to masonry. *International journal for numerical methods in engineering,* 85: 1177–1206.

Oliveira, D. V. and P. B. Lourenço 2004. Implementation and validation of a constitutive model for the cyclic behaviour of interface elements. *Computers & structures*, 1451–1461.

Oliver, J., Huespe, A. E., and Cante, J. C. 2008. An implicit/explicit integration scheme to increase computability of non-linear material and contact/friction problems. *Computer Methods in Applied Mechanics and Engineering*, 197: 1865-1889.

Panian, R., M. Yazdani. 2020. Estimation of the service load capacity of plain concrete arch bridges using a novel approach: Stress intensity factor. *Structures*, 27:1521-1534.

Pelà, L., M. Cervera, and P. Roca. 2011. Continuum damage model for orthotropic materials: Application to masonry. *Computer Methods in Applied Mechanics and Engineering*, 917-930.

Pelà, L., M. Cervera, and P. Roca. 2013. An orthotropic damage model for the analysis of masonry structures. *Construction and Building Materials*, 957–967.

Pelà, L., M. Cervera, S. Oller, and M. Chiumenti. 2014, A localized mapped damage model for orthotropic materials. *Engineering Fracture Mechanics*, 124-125.

Petracca, M., L. Pelà, R. Rossi, S. Oller, G. Camata, and E. Spacone. 2016. Regularization of first order computational homogenization for multiscale analysis of masonry structures. *Computational Mechanics,* 57:257-276.

Petracca, M., L. Pelà, R. Rossi, S. Oller, G. Camata, and E. Spacone. 2017. Multiscale computational first order homogenization of thick shells for the analysis of out-of-plane loaded masonry walls. *Computer Methods in Applied Mechanics and Engineering*, 315: 273-301.

Petracca, M., L. Pelà, R. Rossi, S. Zaghi, G. Camata, and E. Spacone. 2017. Micro-scale continuous and discrete numerical models for nonlinear analysis of masonry shear walls. *Construction and Building Materials*, 149:296-314.

Quinteros, R. D., S. Oller and L. G. Nallim. 2012. Nonlinear homogenization techniques to solve masonry structures problems. *Composite Structures*, 94: 724–730.

Saloustros, S., M. Cervera. and L. Pelà. 2018. Tracking multi-directional intersecting cracks in numerical modelling of masonry shear walls under cyclic loading. *Meccanica*, 53(7), 1757-1776.

STKO Scientific ToolKit for OpenSees. https://asdeasoft.net/stko/

Wu, J. Y., J. Li, and R. Faria. 2006. An energy release rate-based plastic-damage model for concrete. *International Journal of Solids and Structures*, 43:583-612.

Yazdani, M., H. Habibi. 2021. Residual Capacity Evaluation of Masonry Arch Bridges by Extended Finite Element Method. *Structural Engineering International*, 1-12.

Zucchini, A. and P. B. Lourenço. 2002. A micro-mechanical model for the homogenisation of masonry. *International Journal of Solids and Structures*, 39: 3233–3255.

Zucchini, A. and P. B. Lourenço. 2009. A micro-mechanical homogenisation model for masonry: Application to shear walls. *International Journal of Solids and Structures*, 46: 871–886.